Materials Research Proceedings 41 (2024) 1399-1407 https://doi.org/10.21741/9781644903131-155

Sensor integration for process control in deep drawing

JUNG Robert Oliver[1,a *], SEPER Christoph[2,b], JURICEK Christian[2,c] and BLEICHER Friedrich[1,d]

[1]Institute for Production Engineering and Photonic Technologies, TU Wien, Franz Grill Straße 4, Object OA, Vienna 1030, Austria

[2]MAGNA Cosma, Puchberger Straße 267, Weikersdorf 2722, Austria

[a]jung@ift.at, [b]christoph.seper@magna.com, [c]christian.juricek@magna.com, [d]bleicher@ift.at

Keywords: Sheet Metal Forming, Deep Drawing, Control, Sensor Integration

Abstract. In the context of increasing resource efficiency and profitability, deep drawing can be improved using a digital twin and closed-loop process control. Cyber-physical production systems (CPPS) enable data capture and analysis for an autonomous optimization of the manufacturing process. In this work reference sensor signals are used to control the force and material flow with hydraulic actuators between the blank holder and the die. A novel model-based optimization method is proposed to determine the best sensor location, allowing for standardized evaluation and reduced integration time. FE simulations and forming trials are conducted for validation. The findings indicate time and resource savings through an efficient sensor implementation in deep drawing tools for process control.

Introduction

In the European Union (EU), 2.4 million jobs are directly dependent and approximately 12.9 million jobs are overall connected to the automotive industry [1]. In 2021, the EU invested a total of 59.1 billion euros in research and development (R&D) in the automotive sector, which corresponds to 31 % of their overall R&D expenditures [1]. The revenue generated from the automotive industry for the EU amounted to 392.2 billion euros in 2022 [1], which highlights the significance of this fiercely competitive industry sector. Approximately two-thirds of a vehicle body is manufactured using forming technology with deep drawing being the primary method employed. However, the processing window narrows as a result of lightweight construction and the demand for complex geometries. To widen the processing window as well as to enhance resource efficiency and cost-effectiveness, CPPS are required. A categorization of CPPS for deep drawing processes can be realized in different ways. One approach divides them based on the manufacturing technology, namely tandem press setups and single-press setups with transfer and progressive dies [2]. Another approach classifies them based on the computation time of the algorithm. The model based analysis can happen *after*, *during*, or - at the most advanced stage - *before* the stroke. In [3] the algorithm predicts the optimal process parameters for the next stroke *after* a measured stroke. Investigations on control of the material flow in real-time *during* the measured stroke can be found in [4]. A prediction of the optimal process parameters *before* the forming for each blank individually based on the mechanical properties of the incoming material is presented in [5]. For regulating the material flow during the stroke, hydraulic actuators between the blank holder and the die can be used in order to control the material inflow in the flange area based on the stresses in the punch, die and blank holder. Previous investigations can be found in [2], and a general overview of closed-loop control of product properties in metal forming in [6]. Further, [7] provides a comprehensive overview of smart tooling for metal forming, which includes a dedicated chapter on smart tooling with embedded sensors. A crucial aspect for a successful process control during the stroke is to obtain high-quality information about the current

process state, driven by the positioning and type of the sensor. To avoid an iterative experimental evaluation based selection of the location in the tool, a defined methodological approach is proposed in this work.

Methodological approach

The methodological approach to optimize the sensor integration in deep drawing tools for process control is illustrated in Fig. 1. The process starts with the identification of a tool. Next, a finite element (FE) simulation is performed for both a good part and a defective part with splits or wrinkles to evaluate the differences in the simulation outcomes.

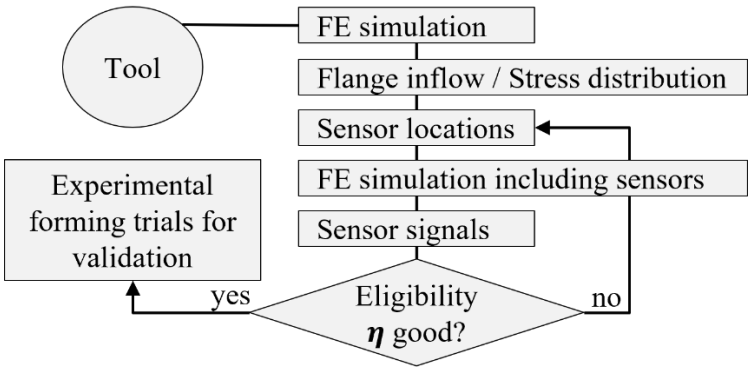

Fig. 1 - Methodological approach to optimize the sensor integration in deep drawing tools for process control during the stroke

Subsequently, the differences in the simulation results provide initial indications at which positions in the tool measurements could be performed. Furthermore, the simulation results help to select the sensor types based on the specific measurement variables. In particular, the implementation of a flange inflow sensor at the location of maximum inflow difference between good and defective parts as well as the implementation of force sensors at the locations of maximum difference in the stress distribution in the tool have been chosen as being appropriate for the application of the respective use case. However, other types of sensors with different physical measurement principles are also considered in the presented approach. Afterwards, the simulation of the good and defective parts needs to be performed again, as the sensor implementations, including milled pockets for assembly and cable routing, influence the stiffness of the tool components. This results in simulated sensor signals, which allows for the calculation of the eligibility η. In this work η represents the suitability of a sensor in a deep drawing tool for control during the stroke, allowing for the classification of process reliability as a Fig. of merit. The procedure for the calculation is explained in a later section. After interpreting the results, a decision is made on whether this process needs to be iteratively repeated or not. The sensor with the highest value for η is physically implemented in the tool, and practical forming experiments are conducted. Ideally, the experimental and simulated results, such as flange draw-in and sheet thinning, coincide, thereby validating the simulation. In this study, the new methodological approach is validated alongside the simulation by implementing and testing the selected sensor in an industrial relevant tool setup.

FE Simulation

Nowadays, FE simulation is indispensable in the design of forming processes. It is also an essential component for the sensor integration presented in this study, as it allows for the simulation of sensor curves, which are subsequently used as input for the calculation of η. LS-DYNA is used in this work and the blank is modeled using shell elements (fully integrated shell DynaType 16 with 7 integration points through the thickness). The element edge length in the sheet is constant and measures 1.5 mm. The tool is modeled using rigid body surfaces with locally refined meshing at

the radii. Elastic volume elements are used to model the stresses in the tool at the sensor positions. The volume of tool inserts is represented by SOLID TET linear with an element edge length of approximately 3 mm and locally refined radii. Coulomb friction model with a constant friction factor of $\mu = 0.1$ is used [8]. Dynamic friction with pressure and velocity dependency was also tested but proved to be ineffective. The Barlat89 material model (LS-DYNA Mat36 - *MAT_3-PARAMETER_BARLAT) is used to model sheet materials with anisotropic properties under plane stress conditions [9]. The used material 1.0952 [10] is cold rolled, has the chemical composition shown in Table 1 and is coated with 50 g/m^2 of zinc at each side.

Table 1 – Chemical composition of 1.0952 in mass-%

C	Si	Mn	P	S	Ti	V	Cr	Ni	Cu	Mo
0.120	0.500	0.600	0.100	0.045	0.300	0.004	0.019	0.137	0.009	0.002

Tensile tests are conducted at 0°, 45°, and 90° to the rolling direction for calibration [11]. The extrapolation of the flow curve is performed using a combination of Swift [12] and Hockett-Sherby [13]. Sheet failure is represented using the Müschenborn-Sonne Forming Limit Diagram (MSFLD) [14].

In the simulation, a decreasing blank holder force (BHF) profile represents a good part, while a constant BHF of 250 kN represents a defective part. After comparing the simulation results, a defect in the form of critical sheet thinning leading to a split is detected on the front side with a constant BHF of 250 kN, see Fig. 2.

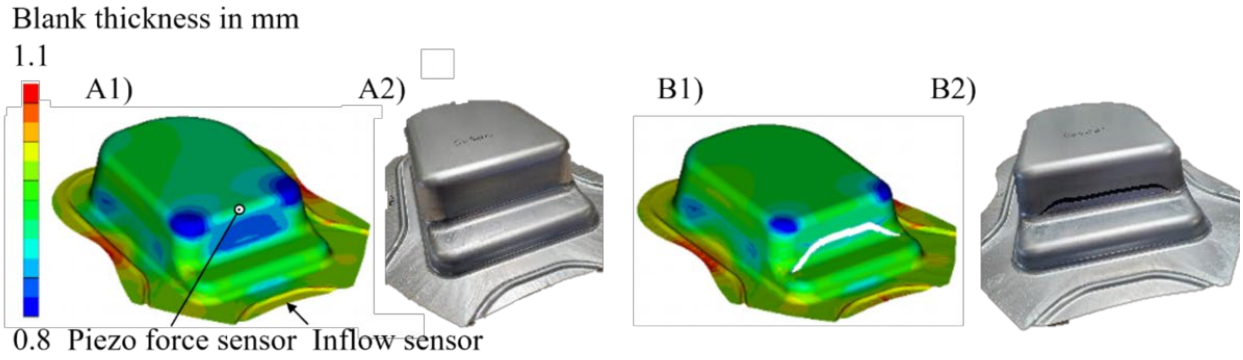

Fig. 2 - Sensor locations and blank thickness in mm of a 1) FE simulated and 2) formed part with A) decreasing BHF profile and B) BHF constant 250 kN

To indirectly measure this split on the flange, a mechanical inflow sensor is used. This sensor consists of a metal blade that can slide through a groove in the blank holder and is permanently pressed against the sheet edge by a pneumatic cylinder. To identify a suitable position for a piezo force sensor, the stress distributions in the tool are analyzed by subtracting the simulation results of the good part from the defective part. The upper punch radius, as marked in Fig. 2, is identified as a potential suitable position for the piezo force sensor. The component geometry is based on a wheelhouse. Recesses in the tool are implemented in the FE simulation to accommodate the installation and cable routing of the two sensors. The new setup is then simulated again.

Eligibility η

In order to explain the general procedure for calculating η, an example is provided for the two selected sensors. The eligibility is defined as the factor describing the necessary qualities or satisfying necessary conditions [15]. In this work, the eligibility η is a defined feature that represents the suitability of a sensor in a deep drawing tool for control during the stroke. It considers cause and effect and is a criterion that allows the classification of process reliability as

a Fig. of merit. The values for the η-parameter range from 0 to 10. However, it is not possible to generalize up to which order of magnitude η can be identified as good or bad. This is because the component geometry, drawing depth, and material strongly influence the calculation. A comparison of η between different tools is therefore not meaningful. Despite of these basic conditions, an absolute comparison of sensors and their positions within a specific deep drawing tool is possible. In the calculation of η, three variables are considered, as represented in Eq. 1.

$$\eta = \frac{5}{2}\,(2T + D + F) \tag{1}$$

The time parameter $\boldsymbol{T}$ is doubly weighted compared to the distance parameter $\boldsymbol{D}$ and the failure condition parameter $\boldsymbol{F}$ as it is the most crucial. The multiplication of the term by 2.5 scales the value range to $\boldsymbol{W_\eta = [0; 10]}$. Eq. 2 illustrates how the time parameter is derived. $\boldsymbol{T}$ describes how early a defect in the sensor curve becomes apparent. Specifically, this parameter represents, when the absolute sensor value curve of the defective component deviates the first time from that of the good component by more than one eighth of magnitude. In this case, the sensor curve of the good component is considered 100 %. An early occurrence of this deviation is preferred as it provides more time to adjust the process by adapting the BHF.

$$T = \frac{s_{12.5}}{s_f} \tag{2}$$

s_f represents the forming stroke from starting point of forming until end of stroke. For instance, if the forming occurs between 280 and 400 mm, with 400 mm total stroke corresponding to Bottom Dead Center (BDC), then s_f would be 120 mm. $s_{12.5}$ represents the displacement at which the deviation between the curves exceeds 12.5 % for the first time. As a result, T approaches 1 when the deviation occurs immediately. Conversely, when the deviation happens closer to BDC, T approaches 0. In this work, the sensors signals are analyzed with respect to the ram slide and thus becomes independent from cycle time. When plotting the sensor signal against time, the x-axis varies depending on the strokes per minute (SPM). The actual critical reaction time required to prevent defects through countermeasures depends on factors such as sensor sampling rate, processor cycle time, and program execution time. Experimental forming trials are performed to indicate whether the control system as a whole will operate effectively. The calculation of the distance parameter D is explained in Eq. 3 and 4. Essentially, the sensor signal of the defective component y_b is divided by the sensor signal of the good component y_g, both measured at one quarter of s_f before BDC.

$$D = \left|\frac{y_b}{y_g} - 1\right|, \; if \;\; |y_b| < |2y_g| \tag{3}$$

$$D = 1, \;\; if \;\; |y_b| \geq |2y_g| \tag{4}$$

If y_b is significantly smaller than y_g, the fraction term approaches 0, resulting in the entire term approaching 1. To ensure that this equation works for both, positive and negative sensor signals, e.g., positive flange inflow or negative stress (compression), the absolute value of D is taken. If y_b is significantly larger than y_g, the term theoretically converges to infinity and would exceed by far T and F. This typically does not occur in flange draw-in but can happen if a part splits and the compressive stress in the tool abruptly drops to 0. Therefore, Eq. 4 is used when the absolute value of y_b is twice as large as the absolute value of y_g, which limits the value range of D to $W_D = [0; 1]$. The failure condition parameter F is selected based on the severity of the defect. This is

necessary, because an early significant difference between two sensor curves can result from large cracks or wrinkles. The challenge lies in obtaining a significant difference in the sensor curves for the onset of necking or wrinkling. Fig. 3 shows an example subdivision of the defect appearance considering cracks.

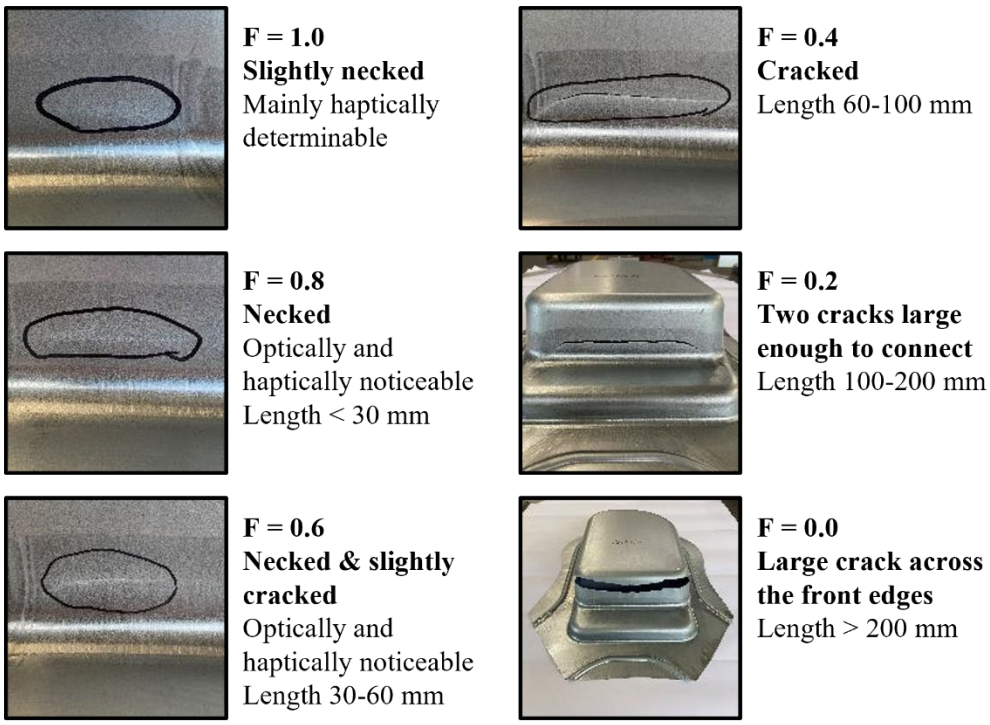

Fig. 3 - Classification of component quality with regard to crack formation for the failure condition parameter F

In the following, an exemplary determination of η for the simulated intake sensor at the flange and the simulated piezo force sensor in the punch is presented. The quality condition of the component in the final step of the FE simulation is compared with the classification shown in Fig. 3, and thus F = 0.2 is selected. The variables y_g and y_b are measured a quarter of s_f before BDC. Since s_f is 120 mm, y_g and y_b are measured 30 mm before BDC. The results are based solely on the FE simulation and η is calculated for the intake and piezo force sensor, as shown in Table 2.

Table 2 - Results of $\boldsymbol{\eta}$ for intake and piezo force sensor

	$s_{12.5}$	y_g	y_g	T	D	F	$\boldsymbol{\eta}$
Intake sensor	21.55 mm	30.96 mm	28.85 mm	0.18	0.07	0.20	**1.57**
Piezo force sensor	47.96 mm	-866.55 pC	-993.68 pC	0.40	0.15	0.20	**2.87**

The two sensor signals are plotted over the ram slide in Fig. 4 and Fig. 5. Additionally, the calculated parameters and the crack initiation of the defective part are marked. Since η is higher for the piezo force sensor than for the intake sensor, the piezo force sensor is implemented for control purpose.

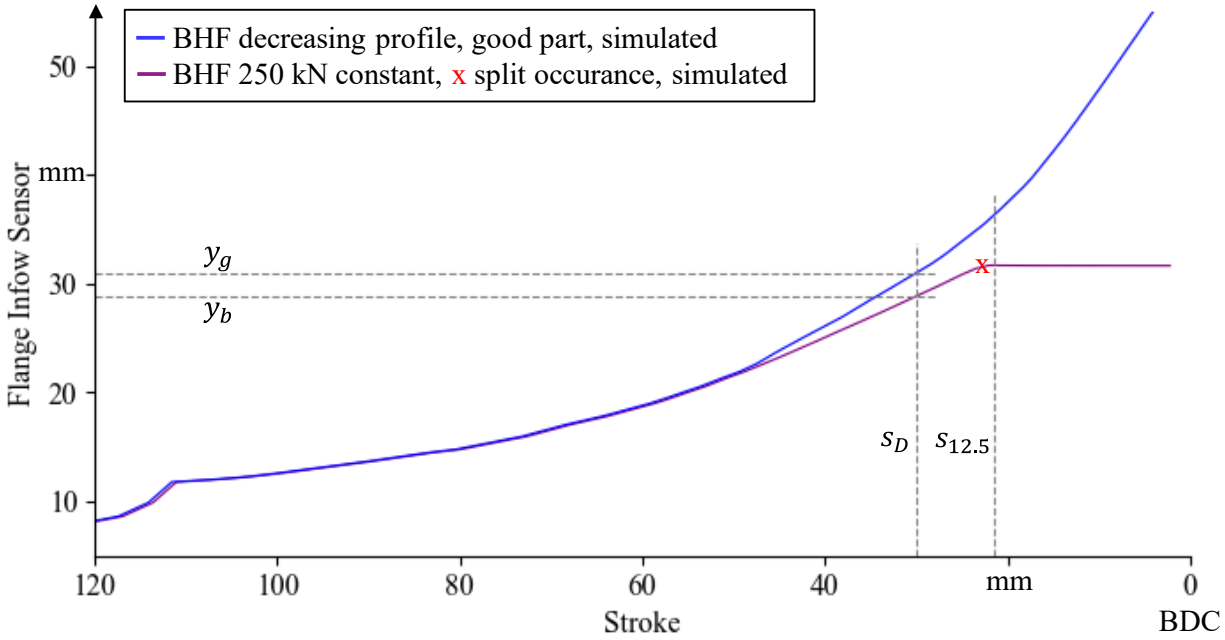

Fig. 4 - Material inflow signals based on FE simulation and variables for determination of eligibility $\boldsymbol{\eta}$

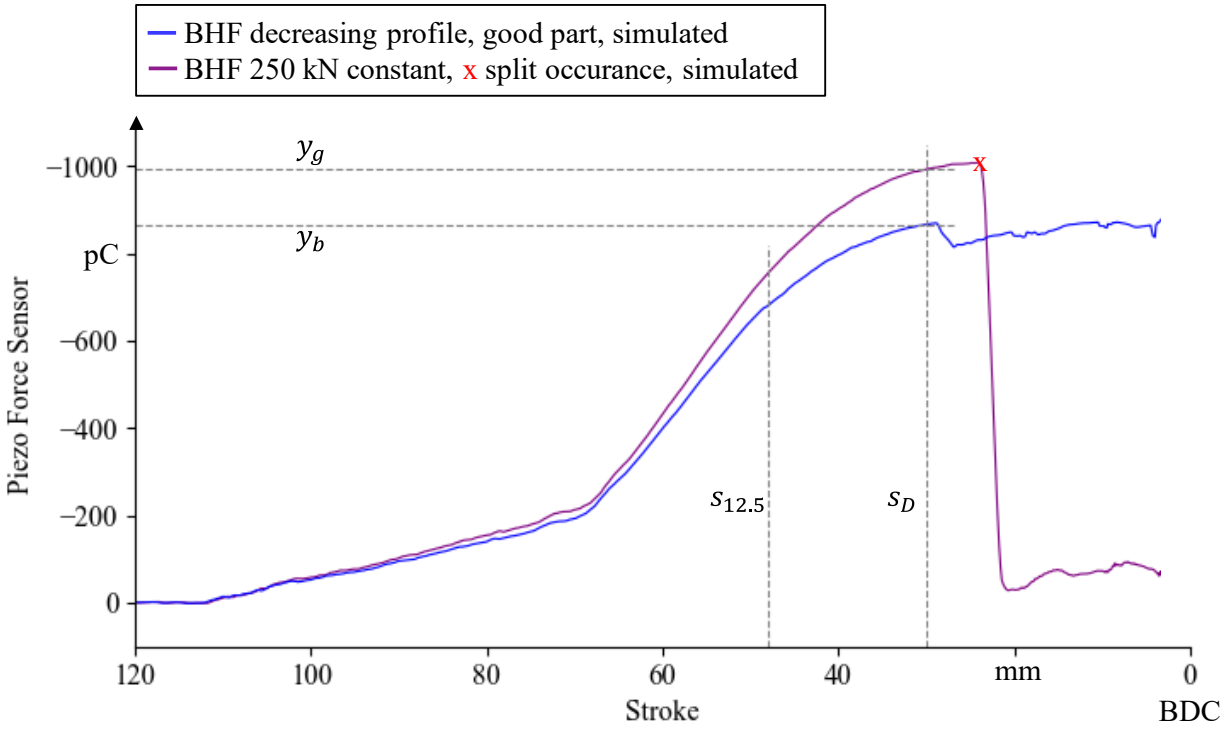

Fig. 5 – Piezo force sensor signals based on FE simulation and variables for determination of eligibility $\boldsymbol{\eta}$

Experimental forming trials with quality control during the stroke

In Fig. 6, simulated (blue and purple) and experimentally determined signals (red, green and black) of the piezo force sensor are plotted in pC over the ram slide in mm. The magnitude of the signal decreases as the pressure-induced stresses in the punch increase. Comparing the purple curve, representing a simulated split, with the three red curves, representing experimental splits, it reveals

that the simulation closely matches reality. However, in the simulation, the tension in the sensor element abruptly drops to zero at the onset of cracking, which is not observed in the experimental tests. Here, the stress distribution in the tool appears to be more homogeneous. By adjusting the failure model of the FE simulation, the real behavior of the component could be captured even more accurately. The blue curves, representing the simulated good part, and green curves, representing the experimental good parts, also closely match, until a tension drop can be identified in the simulated good parts at approximately 30 mm before BDC. It should be noted that the FE simulation is only an approximation of the real deep drawing process, as many simplified assumptions are made, such as the idealized geometry of the tool and blank, constant friction, and excluded inaccuracies in the determined material properties. Furthermore, the portion of the simulated sensor curves that deviates from the experimentally determined sensor curves does not affect the calculation of η, as all relevant values are extracted only from the matching region before the simulated sensor curves exhibit a sudden tension drop.

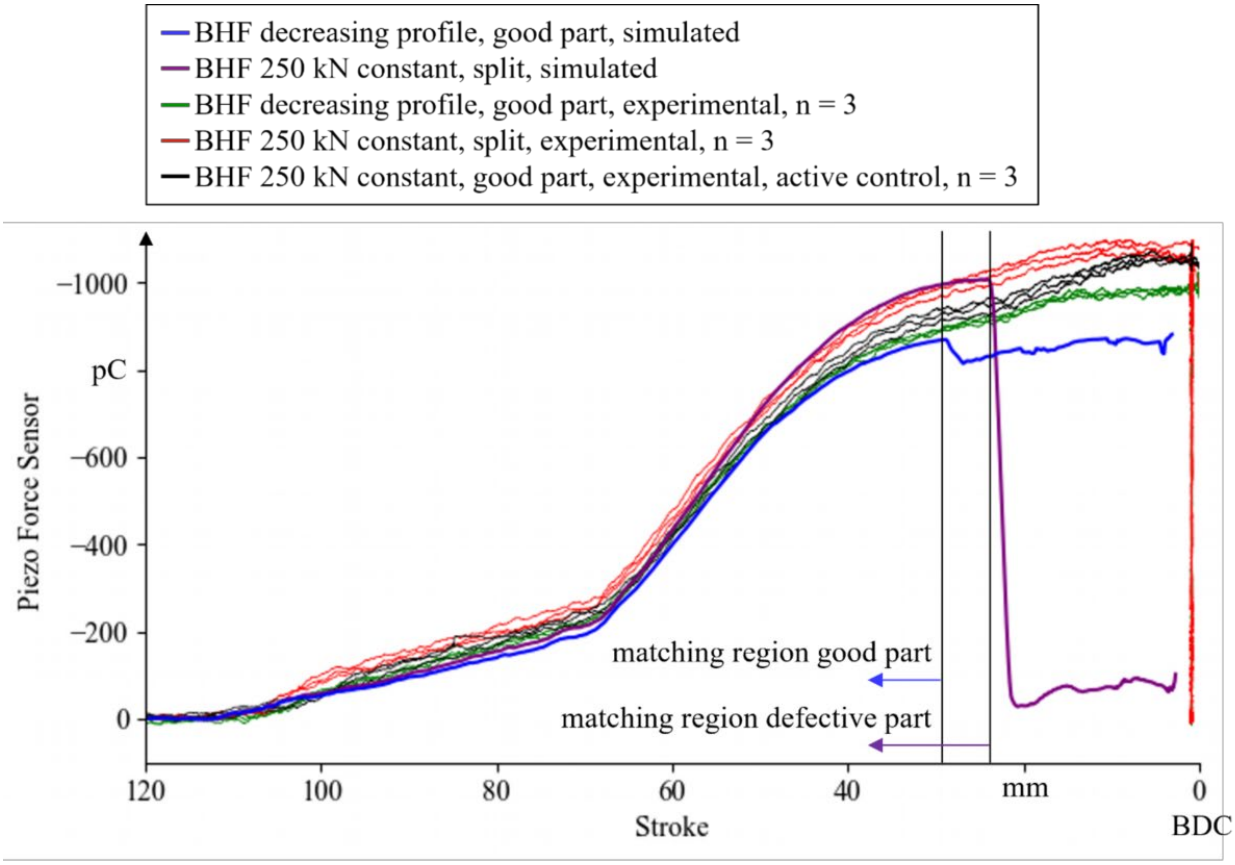

Fig. 6 – Comparison of piezo force sensor signals: FE simulation, experimental forming trials without control, and with control

The black curve represents the sensor signal from the experiment where the BHF is set to defective part settings (250 kN constant causing splits), but a control with the piezo force sensor and hydraulic actuators between the blank holder and die is active. Up to 30 mm before BDC, the sensor signal aligns with the green and good part curves. However, as the pressure stresses near the sensor curves of the defective parts at around 5 mm before BDC, a deviation between the good parts with active control and 250 kN constant BHF and the good parts without active control but a decreasing BHF profile becomes evident. The only distinguishing factor between the parts represented by the red sensor curves and those represented by the black curves is the presence of active control. The red parts exhibit a significant split across the front and are considered scrap,

whereas the black parts are of good quality. Two PID controllers are used. The higher-level control loop regulates the current sensor data to the reference sensor data of a good part by adjusting the pressure in the hydraulic actuators between the blank holder and the die. The second control loop regulates the actual pressure of the actuators to the desired pressure. The η-value for the piezo force sensor is higher than for the draw-in sensor and the control with the piezo force sensor is successfully implemented. The additional use of the draw-in sensor signal offers an alternative solution of single sensor signal implementation. In general, it is recommended to consider more than one single sensor source by the sensor fusion approach. The presented model is basically aimed at identifying the optimal sensor position.

Summary and future directions

This new methodological approach allows for improving sensor integration for the control of deep drawing processes during the stroke. It is achieved by a combination of FE simulation and assessment of results by calculation of sensor eligibility η. Initially, the differences between good parts and defective parts are identified using FE simulation. The required types of sensors are derived from this analysis. In the experimental set-up and by the selected testing specimen used in this study, this resulted in the selection of a mechanical inflow sensor at the front end of the component and a piezoelectric force sensor in the punch. The area depicted in Fig. 3 is referred to as the front. Subsequently, the sensors, including all necessary mountings and cable routing, are implemented in the FE simulation. The sensor eligibility η, which is defined to consider cause and effect issues, is calculated for the simulated sensor curves. This metric takes into account, how early and how sensitively the sensor detects the occurrence of a component defect, considering both, the sensor's response magnitude and the severity of the defect. Finally, the sensor with the highest η value is implemented in the process control, resulting in successful crack avoidance. A close agreement between the simulated sensor curves and the experimental results is a prerequisite. This approach not only accelerates sensor integration by the use of process modelling but also provides the opportunity to select sensor positions according to quantitative measures. However, the comparison between η values is only valid within one tool. Different tools can significantly influence the calculation of η due to variations in friction, drawing depths, geometries, and materials. It is possible that a defect may occur late in the stroke, close to the bottom dead center, without any prior indication through changes in, for example, flange inflow speed or tool stresses. In such cases, implementing control during the stroke may be challenging, and the proposed approach may have limitations.

The formed components of a vehicle body should be clustered, and a unified table for the failure condition parameter F should be created for each cluster, minimizing the user's discretion. The significance of the presented Fig. of merit should be ensured through additional deep drawn components. Furthermore, in the future, attempts should be made to train artificial intelligence to correlate the sensor signals and η by visually detectable effects on the component. Through this approach, a continuous automatic output of F and an increased process understanding would be conceivable. Integrating the assessed model directly into the FE simulation software would be desirable to enhance usability and eliminate the need for switching between different software tools.

Acknowledgment

The authors thank the MAGNA Cosma R&D Team and the Institute of Production Engineering and Photonic Technologies (IFT) of TU Wien for their support in terms of scientific and technical expertise. Special appreciation to MAGNA Cosma for funding of this research project.

References

[1] S. de Vries, The Automobile Industry - Pocket Guide 2023/2024, ACEA - European Automobile Manufacturers' Association (2023) 5-9.

[2] R.O. Jung, F. Bleicher, S. Krall, C. Juricek, R. Lottes, K. Steinschütz, T. Reininger, Cyber Physical Production Systems for Deep Drawing, J. Manuf. Sci. Eng. 145 (2023) 101006. https://doi.org/10.1115/1.4062903

[3] S. Thaddaeus, P. Henri, Adjustable Balancing Block for Closed Loop Die Control, Patent WO2021141819A1. (2021).

[4] M. Barthau, M. Liewald, New approach on controlling strain distribution manufactured in sheet metal components during deep drawing process, International Conference on the Technology of Plasticity, Procedia Engineering. 207 (2017) 66-71. https://doi.org/10.1016/j.proeng.2017.10.740

[5] H. Kim, J.C. Gu, L. Zoller, Control of the servo-press in stamping considering the variation of the incoming material properties, International Deep Drawing Research Group 38th Annual Conference, IOP Conference Series: Materials Science and Engineering. 651 (2019) 012062. https://doi.org/10.1088/1757-899X/651/1/012062

[6] J.M. Allwood, S.R. Duncan, J. Cao, P. Groche, G. Hirt, B. Kinsey, T. Kuboki, M. Liewald, A. Sterzing, A.E. Tekkaya, Closed-loop control of product properties in metal forming, CIRP Annals - Manufacturing Technology. 65 (2016) 573-596. https://doi.org/10.1016/j.cirp.2016.06.002

[7] J. Cao, E. Brinksmeier, M. Fu, R.X. Gao, B. Liang, M. Merklein, M. Schmidt, J. Yanagimoto, Manufacturing of advanced smart tooling for metal forming, CIRP Annals - Manufacturing Technology. 68 (2019) 605-628. https://doi.org/10.1016/j.cirp.2019.05.001

[8] C.A. Coulomb, Théorie des machines simples: en ayant égard au frottement de leurs parties, et à la roideur de cordages, Mémoires de mathématique et de physique, 1785

[9] F. Barlat, K. Lian, Plastic behavior and stretchability of sheet metals. Part I: A yield function for orthotropic sheets under plane stress conditions, International Journal of Plasticity. 5 (1989) 51-66. https://doi.org/10.1016/0749-6419(89)90019-3

[10] DIN EN 10027-2: Bezeichnungssysteme für Stähle - Teil 2: Nummernsystem. Beuth Verlag GmbH, 2015

[11] DIN EN ISO 6892-1: Metallische Werkstoffe - Zugversuch - Teil 1: Prüfverfahren bei Raumtemperatur. Beuth Verlag GmbH, 2020

[12] H.W. Swift, Plastic instability under plane stress, Journal of the Mechanics and Physics of Solids. 1 (1952) 1-18. https://doi.org/10.1016/0022-5096(52)90002-1

[13] J.E. Hockett, O.D. Sherby, Large strain deformation of polycrystalline metals at low homologous temperatures, Journal of the Mechanics and Physics of Solids. 23 (1975) 87-98. https://doi.org/10.1016/0022-5096(75)90018-6

[14] W. Müschenborn, H.-M. Sonne, Einfluß des Formänderungsweges auf die Grenzformänderungen des Feinblechs, Archiv für das Eisenhüttenwesen. 46 (1975) 597-602. https://doi.org/10.1002/srin.197503686

[15] Information on https://dictionary.cambridge.org/de/worterbuch/englisch/eligibility (last checked 5th of February, 2024)